IEEE Access
Multidisciplinary | Rapid Review | Open Access Journal

Received July 24, 2018, accepted August 22, 2018, date of publication August 30, 2018, date of current version September 21, 2018.

Digital Object Identifier 10.1109/ACCESS.2018.2867899

Rotor Position Sensorless Control of Wound-Field Flux-Switching Machine Based on High Frequency Square-Wave Voltage Injection

HONG QUAN NGUYEN AND SHENG-MING YANG, (Member, IEEE)
Department of Electrical Engineering, National Taipei University of Technology, Taipei 10608, Taiwan
Corresponding author: Sheng-Ming Yang (smyang@ntut.edu.tw)

This work was supported by the Ministry of Science and Technology, Taiwan, under Grant MOST 107-2221-E-027-082-MY3.

ABSTRACT This paper compares three shaft-sensorless control schemes for wound-field flux-switching machines based on a high frequency (HF) square-wave voltage injection technique. An HF model for the machine, with inclusion of the field winding, is first presented. Because the machine had armature and field windings, HF voltage is injected into and processed in the armature winding as with conventional permanent magnet synchronous machines (PMSMs) or injected into one winding and processed in the induced current signal in the other winding. Both the analytical and experimental results reveal that the scheme with d-axis voltage injection and a q-axis induced current process is generally similar to that used for PMSMs. Polarity identification is required to prevent phase errors in the estimated position. The schemes with separate windings for voltage injection and current processing demonstrate superior performance compared with the scheme without, and both schemes do not require polarity identification. Moreover, voltage injection at the field winding has an additional advantage for high-speed operations.

INDEX TERMS Wound-field flux switching machine, polarity detection, sensorless control, square-wave voltage injection.

I. INTRODUCTION

Shaft-sensorless control techniques have been extensively developed and applied for permanent magnet synchronous machines (PMSMs), especially saliency-based algorithms [1]–[15]. Eliminating the position sensor not only increases system reliability but also reduces system volume, cost, and noise effects. Among the existing methods, schemes based on high frequency (HF) voltage injection are particularly suited for standstill and low-speed applications. These algorithms are divided into three groups: 1) rotating voltage injection: extracts rotor position through injection of a rotating voltage vector in both d- and q-axes on a stationary reference frame [2]–[4]; 2) pulsating voltage injection: injects a carrier voltage into either d- or q-axis in the rotor reference frame [5]–[7]; and 3) square-wave voltage injection: injects a square voltage in either d- or q-axis in the rotor reference frame [8]–[11]. The methods in the last group have demonstrated a larger position and speed-loop bandwidth than the other methods [8]. However, polarity identification is required for the aforementioned methods because the induced HF current has two cycles per electrical period [12]–[14]. Several polarity identification methods have been proposed; these are classified into two types according to whether or not carrier signals are added. The first type is based on amplitude variation due to stator iron saturation [12] and the second type utilizes the secondary current harmonic or zero sequence carrier voltage [13], [14]. The first type is simpler and has a larger signal-to-noise ratio than the second, but the second type has a faster convergence rate than the first.

The flux-switching machine (FSM) is a relatively new class of motor that has gained considerable research attention. Among various FSM topologies, the wound-field FSM (WF-FSM) is low cost, appropriate for harsh environments, and is easy to regulate fields under relatively high operating speeds or relatively large starting torque [16]–[18]. Because of the similarity of the operational principle, the conventional vector control and HF voltage injection methods developed for PMSMs can also be employed for controlling FSMs [19], [20]. WF-FSM has armature and filed windings; this leads to the possibilities of injecting and processing HF signals into the armature winding, as with

conventional PMSMs, or injecting and processing HF signals into separate windings.

This paper compares three schemes for motor position estimation and shaft-sensorless control with HF square-wave voltage injection for WF-FSM: 1) voltage injection along the d-axis, and the induced q-axis current is processed, 2) voltage injection along the q-axis and the induced field current is processed, and 3) voltage injection into the field and the induced q-axis current is processed. Implementation of the rotor position estimation with these schemes is analyzed, and their performances are then evaluated experimentally.

II. MATHEMATICAL MODEL FOR WF-FSM

A. FUNDAMENTAL FREQUENCY MODEL

The WF-FSM investigated in this study is a three-phase, external rotor machine with 24-stator slots and 14-rotor poles. Fig. 1 presents a cross section of the machine, and Table 1 lists its parameters. Details on the design and performance of this machine can be found in [18].

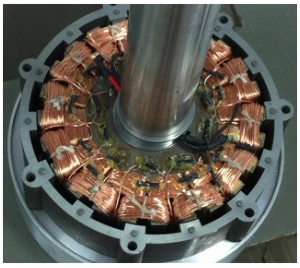

FIGURE 1. Cross section of the 24-stator slot, 14-rotor pole WF-FSM.

TABLE 1. Parameters of the WF-FSM.

Parameters	Quantity	Units
Stator slot/ Rotor pole	12/14	-
Rated speed	600	rpm
Rated torque	5.70	Nm
Armature Phase resistance	2.52	Ω
Field winding resistance	5.36	Ω
q-axis inductance	13.32	mH
d-axis inductance	14.56	mH
Field winding self-inductance	36.02	mH
Mutual inductance	9.60	mH

The voltage of the armature windings of the WF-FSM can be derived based on the model for conventional PMSMs. The phase voltage of the armature windings are expressed as follows:

$$\begin{bmatrix} v_{as} \\ v_{bs} \\ v_{cs} \end{bmatrix} = r_s \begin{bmatrix} i_{as} \\ i_{bs} \\ i_{cs} \end{bmatrix} + s \begin{bmatrix} \lambda_{as} \\ \lambda_{bs} \\ \lambda_{cs} \end{bmatrix} \tag{1}$$

where r_s is the phase resistance, v_{as}, v_{bs}, and v_{cs} are phase voltages, i_{as}, i_{bs}, i_{cs}, are phase currents, and λ_{as}, λ_{bs}, and λ_{cs} are the flux linkages. The symbol "s" denotes the differential operator. Self-inductance are modeled to include leakage inductance L_{ls}, DC component L_{0s}, and AC component L_{2s} as

$$\begin{aligned} L_{as,as} &= L_{ls} + L_{0s} - L_{2s}\cos(2\theta_r) \\ L_{bs,bs} &= L_{ls} + L_{0s} - L_{2s}\cos(2\theta_r - 2\pi/3) \\ L_{cs,cs} &= L_{ls} + L_{0s} - L_{2s}\cos(2\theta_r + 2\pi/3) \end{aligned} \tag{2}$$

Mutual inductances between phase windings are given as

$$\begin{aligned} M_{as,bs} &= M_{bs,as} = -1/2L_{0s} - L_{2s}\cos(2\theta_r + 2\pi/3) \\ M_{bs,cs} &= M_{cs,bs} = -1/2L_{0s} - L_{2s}\cos(2\theta_r) \\ M_{cs,as} &= M_{as,cs} = -1/2L_{0s} - L_{2s}\cos(2\theta_r - 2\pi/3) \end{aligned} \tag{3}$$

The armature flux linkages are presented in terms of matrix as follows:

$$\begin{bmatrix} \lambda_{as} \\ \lambda_{bs} \\ \lambda_{cs} \end{bmatrix} = \begin{bmatrix} L_{as,as} & M_{as,bs} & M_{as,cs} \\ M_{bs,as} & L_{bs,bs} & M_{bs,cs} \\ M_{cs,as} & M_{cs,bs} & L_{cs,cs} \end{bmatrix} \begin{bmatrix} i_{as} \\ i_{bs} \\ i_{cs} \end{bmatrix} + \begin{bmatrix} \lambda_{fa} \\ \lambda_{fb} \\ \lambda_{fc} \end{bmatrix} \tag{4}$$

where λ_{fa}, λ_{fb}, and λ_{fc} are the flux linkages from the field winding. With the assumption of symmetrical inductances, these flux linkages can be expressed as

$$\begin{aligned} \lambda_{fa} &= L_{mf}\sin(\theta_r)i_f \\ \lambda_{fb} &= L_{mf}\sin(\theta_r + 2\pi/3)i_f \\ \lambda_{fc} &= L_{mf}\sin(\theta_r - 2\pi/3)i_f \end{aligned} \tag{5}$$

where L_{mf} is the mutual inductance between the field and armature winding, and i_f is the DC field current.

The voltage of the field winding is given as

$$\begin{aligned} v_f &= r_f i_f + sL_{fs}i_f + s[L_{mf}\sin(\theta_r)i_{as} \\ &\quad + L_{mf}\sin(\theta_r + 2\pi/3)i_{bs} + L_{mf}\sin(\theta_r - 2\pi/3)i_{cs}] \end{aligned} \tag{6}$$

where r_f and L_{fs} are the resistance and self-inductance of the field winding, respectively. Equations (4) and (6) are converted to the rotor dq frame, following which the resulting equations are combined. The voltage equation for the WF-FSM can be simplified as

$$\begin{bmatrix} v_{qs}^r \\ v_{ds}^r \\ v_f \end{bmatrix} = \begin{bmatrix} r_s + L_{qs}s & \omega_r L_{ds} & \omega_r L_{mf} \\ -\omega_r L_{qs} & r_s + L_{ds}s & L_{mf}s \\ 0 & (3/2)L_{mf}s & r_f + L_{fs}s \end{bmatrix} \begin{bmatrix} i_{qs}^r \\ i_{ds}^r \\ i_f \end{bmatrix} \tag{7}$$

where ω_r is the electrical speed, v_{qs}^r, v_{ds}^r, v_f and i_{qs}^r, i_{ds}^r, and i_f are the q, d, and field voltages and currents, respectively, and L_{qs}, L_{ds} are the q- and d-axis inductance. L_{qs} and L_{ds} are defined as

$$\begin{aligned} L_{qs} &= 3/2(L_{0s} - L_{2s}) + L_{ls} \\ L_{ds} &= 3/2(L_{0s} + L_{2s}) + L_{ls} \end{aligned} \tag{8}$$

Equation (7) shows that the armature voltages are coupled to the field current, but the field voltage is coupled only to the armature d-axis current.

B. HF MODEL

For frequency much higher than the fundamental frequency, (7) can be simplified as follows:

$$\begin{bmatrix} v^r_{qsi} \\ v^r_{dsi} \\ v_{fi} \end{bmatrix} = \begin{bmatrix} L_{qs}s & 0 & 0 \\ 0 & L_{ds}s & L_{mf}s \\ 0 & (3/2)L_{mf}s & L_{fs}s \end{bmatrix} \begin{bmatrix} i^r_{qsi} \\ i^r_{dsi} \\ i_{fi} \end{bmatrix} \quad (9)$$

where subscript 'i' represents the corresponding HF component. Because all of the inductances in (9) have a differential operator, it can be rewritten as

$$s\begin{bmatrix} i^r_{qsi} \\ i^r_{dsi} \\ i_{fi} \end{bmatrix} = \begin{bmatrix} \frac{1}{L_{qs}} & 0 & 0 \\ 0 & \frac{2L_{fs}}{2L_{ds}L_{fs}-3L^2_{mf}} & \frac{-2L_{mf}}{2L_{ds}L_{fs}-3L^2_{mf}} \\ 0 & \frac{-3L_{mf}}{2L_{ds}L_{fs}-3L^2_{mf}} & \frac{2L_{ds}}{2L_{ds}L_{fs}-3L^2_{mf}} \end{bmatrix} \times \begin{bmatrix} v^r_{qsi} \\ v^r_{dsi} \\ v_{fi} \end{bmatrix} \quad (10)$$

Equation (10) illustrates the relationship between HF winding currents and voltages. This equation is used to analyze the induced current for HF voltage injection at the windings. Three schemes for estimating motor position with HF square-wave voltage injection are presented in the following sections.

III. HF VOLTAGE INJECTION AT THE ESTIMATED D-AXIS

This section analyzes the position estimation scheme with HF voltage injection commonly used in PMSMs. In this scheme, the HF voltage is injected along the d-axis, and the induced q-axis current is used for position estimation [8]. Equation (10) can be rewritten without the field components as

$$s\begin{bmatrix} i^r_{qsi} \\ i^r_{dsi} \end{bmatrix} = \begin{bmatrix} \frac{1}{L_{qs}} & 0 \\ 0 & \frac{2L_{fs}}{2L_{ds}L_{fs}-3L^2_{mf}} \end{bmatrix} \begin{bmatrix} v^r_{qsi} \\ v^r_{dsi} \end{bmatrix} \quad (11)$$

Transform (11) into the estimated rotor reference frame and let $\Delta\theta_r$ be the error between the actual and the estimated rotor position; then, the induced currents in the estimated rotor reference frame can be calculated as

$$s\begin{bmatrix} i^{re}_{qsi} \\ i^{re}_{dsi} \end{bmatrix} = \frac{1}{L_1^2 - L_2^2} \times \begin{bmatrix} L_1 - L_2\cos(2\Delta\theta_r) & L_2\sin(2\Delta\theta_r) \\ L_2\sin(2\Delta\theta_r) & L_1 + L_2\cos(2\Delta\theta_r) \end{bmatrix} \begin{bmatrix} v^{re}_{qsi} \\ v^{re}_{dsi} \end{bmatrix} \quad (12)$$

where 're' indicates that the variable is in the estimated rotor reference frame, and L_1 and L_2 are

$$L_1 = \frac{L_{qs}+L_{ds}}{2} - \frac{3L^2_{mf}}{4L_{fs}}, \quad L_2 = \frac{L_{qs}-L_{ds}}{2} + \frac{3L^2_{mf}}{4L_{fs}} \quad (13)$$

As shown in (12), the induced HF currents are similar to those for typical PMSMs, except L_1 and L_2. By setting $v^{re}_{qsi} = 0$ and v^{re}_{dsi} to a square voltage with magnitude V_{di}, and by replacing the differential currents with difference currents, a current error can be deduced from the induced q-axis current as follows for small $\Delta\theta_r$:

$$\begin{aligned} i_{err\_dq} &= \Delta i^{re}_{qsi} = \frac{L_2}{L_1^2 - L_2^2} V_{di}\Delta T \sin(2\Delta\theta_r) \\ &\cong \frac{2L_2}{L_1^2 - L_2^2} V_{di}\Delta T\,\Delta\theta_r = K_{err\_dq}\Delta\theta_r \end{aligned} \quad (14)$$

where ΔT is the half period of the injection voltage andK_{err_dq} is a factor representing the sensitivity of the current error to the position error. Δi^r_{qsi} in (14) is also denoted as i_{err_dq} for conveniently comparing against other schemes. The last subscript dq indicates that the HF voltage is injected along the d-axis and the armatures q-axis current is processed for position error. K_{err_dq} can also be expressed with L_q and L_d as

$$K_{err\_dq} = \frac{2L_{fs}(L_{qs}-L_{ds}) + 3L^2_{mf}}{L_{qs}(2L_{ds}L_{fs} - 3L^2_{mf})} V_{di}\cdot\Delta T \quad (15)$$

Both the machine saliency level and winding inductances affect K_{err_dq}.

Figure 2 shows the simulated induced current error versus rotor position error with the d-axis voltage injection. Motor parameters are shown in Table 1; ΔT and V_{di} are set to 0.22 ms, and 20 V, respectively, in the simulations. The error signal is sinusoidal and has two cycles per electrical period, which is consistent with the results of (14).

Figure 3 shows the rotor position estimator based on this scheme. The measured q-axis current is processed with a high-pass filter first to separate the fundamental and the HF components. Next, the current difference is calculated and its sign corrected. This yields the current error i_{err_dq}. Finally, a closed loop with a proportional plus integral (PI) regulator forced i_{err_dq} to zero and tracked the rotor position. Because the current error has two cycles per electrical period, correction of the polarity of the estimated rotor position is required to prevent phase errors. Polarity identification procedures similar to those used in PMSMs are used for WF-FSM [21].

Note that the position estimator presented in Fig. 3 does not require any low-pass filters, which are generally used in other HF voltage injection schemes. As a result, the time delay in tracking rotor position is reduced. Therefore, bandwidths of speed controller and position estimators increased and the stability of the system is enhanced.

IV. HF VOLTAGE INJECTION AT THE ESTIMATED Q-AXIS

Injecting HF voltage along either the estimated q- or d-axis of the armature winding induces current in the field winding. The induced field current can be processed for a position error signal. Because the performances of the q- and d-axes are similar, only the voltage injection at the q-axis is investigated

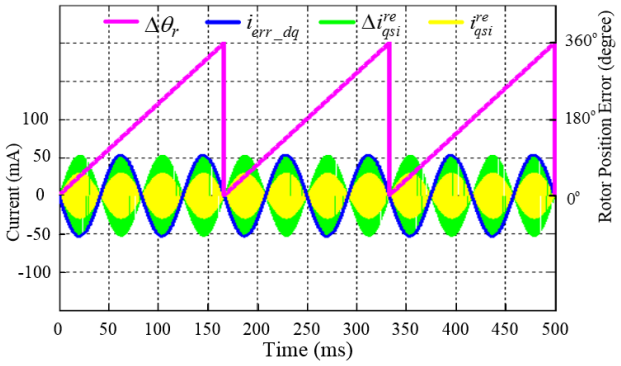

FIGURE 2. Calculated *q*-axis induced current error with the *d*-axis HF voltage injection scheme.

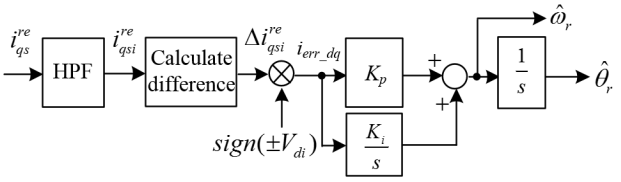

FIGURE 3. Rotor position estimator for the *d*-axis square-wave HF voltage injection.

in this paper. By expressing (10) as the following form and setting v_{fi} to 0, the induced HF field current becomes

$$si_{fi} = \begin{bmatrix} 0 & \dfrac{-3L_{mf}}{2L_{ds}L_{fs} - 3L_{mf}^2} \end{bmatrix} \begin{bmatrix} v^r_{qsi} \\ v^r_{dsi} \end{bmatrix} \tag{16}$$

Transform the voltages to the estimated rotor reference frame; then, the field current can be expressed as

$$si_{fi} = \frac{-3L_{mf}}{2L_{ds}L_{fs} - 3L_{mf}^2} \begin{bmatrix} \sin(\Delta\theta_r) & \cos(\Delta\theta_r) \end{bmatrix} \begin{bmatrix} v^{re}_{qsi} \\ v^{re}_{dsi} \end{bmatrix} \tag{17}$$

Let $v^{re}_{dsi} = 0$ and v^{re}_{qsi} to a square voltage with magnitude V_{qi}. Current errors can be deduced from the induced field current as follows for small $\Delta\theta_r$:

$$\begin{aligned} i_{err\_qf} &= \Delta i_{fi} = \frac{-3L_{mf}}{2L_{ds}L_{fs} - 3L_{mf}^2} V_{qi}\Delta T \sin(\Delta\theta_r) \\ &\cong \frac{-3L_{mf}}{2L_{ds}L_{fs} - 3L_{mf}^2} V_{qi}\Delta T\,\Delta\theta_r = K_{err\_qf}\,\Delta\theta_r \end{aligned} \tag{18}$$

where i_{err_qf} denotes the field current error, and K_{err_qf} is the position error sensitivity factor, and K_{err_qf} is

$$K_{err\_qf} = \frac{-3L_{mf}}{2L_{ds}L_{fs} - 3L_{mf}^2} V_{qi} \cdot \Delta T \tag{19}$$

As shown, K_{err_qf} is negatively proportional to the mutual inductance between the armature and field windings and is independent of the saliency of the machine. The position estimator for the q-axis square-wave voltage injection is identical to the estimator shown in Fig. 3, except that the input to the estimator is i_{fi} and the input to the PI controller is i_{err_qf}. Hence, its block diagram is not presented here.

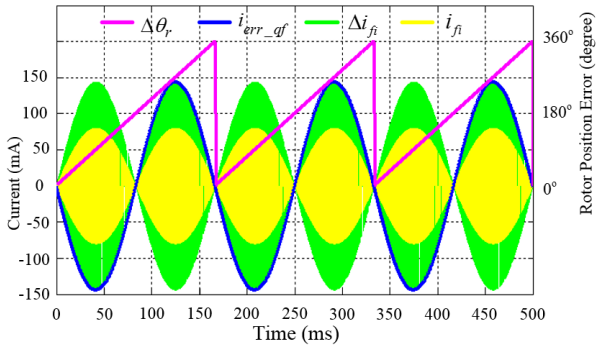

FIGURE 4. Calculated field induced current error with the *q*-axis HF voltage injection scheme.

Figure 4 shows the calculated induced current error versus rotor position error using this scheme. V_{qi} and ΔT are set to the same level as those used in Section III. A noticeable feature of the position error i_{err_qf} waveform is that there is only one cycle per electrical period. Consequently, no polarity identification is required. This property highlights a significant advantage of this scheme. Moreover, comparing the peak value of i_{err_qf} in Fig. 4 and the peak value of i_{err_dq} in Fig. 2, the position error sensitivity of this scheme is significantly higher than the scheme presented in Section III.

V. HF VOLTAGE INJECTION AT THE FIELD WINDING

When the HF voltage is injected into the field winding, the estimated q-axis that induces current is processed for a position error signal. Equation (3) can be rewritten into the following form and by setting v^{re}_{qsi} and v^{re}_{dsi} to zero. The induced armature currents are

$$s \begin{bmatrix} i^r_{qsi} \\ i^r_{dsi} \end{bmatrix} = \begin{bmatrix} 0 \\ \dfrac{-2L_{mf}}{2L_{ds}L_{fs} - 3L_{mf}^2} \end{bmatrix} v_{fi} \tag{20}$$

Then, transform the currents into the estimated rotor reference frame:

$$s \begin{bmatrix} i^{re}_{qsi} \\ i^{re}_{dsi} \end{bmatrix} = \frac{-2L_{mf}}{2L_{ds}L_{fs} - 3L_{mf}^2} \begin{bmatrix} \sin(\Delta\theta_r) \\ \cos(\Delta\theta_r) \end{bmatrix} v_{fi} \tag{21}$$

Next, v_{fi} is set to a square voltage with magnitude V_{fi}. A current error can be deduced from the induced q-axis current as follows for small $\Delta\theta_r$:

$$\begin{aligned} i_{err\_fq} &= \Delta i^{re}_{qsi} = \frac{-2L_{mf}}{2L_{ds}L_{fs} - 3L_{mf}^2} V_{fi}\Delta T \sin(\Delta\theta_r) \\ &\cong \frac{-2L_{mf}}{2L_{ds}L_{fs} - 3L_{mf}^2} V_{fi}\Delta T\,\Delta\theta_r = K_{err\_fq}\Delta\theta_r \end{aligned} \tag{22}$$

where i_{err_fq} is the q-axis current error with the field voltage injection, K_{err_fq} is the position error sensitivity factor, and K_{err_fq} is

$$K_{err\_fq} = \frac{-2L_{mf}}{2L_{ds}L_{fs} - 3L_{mf}^2} V_{fi} \cdot \Delta T \tag{23}$$

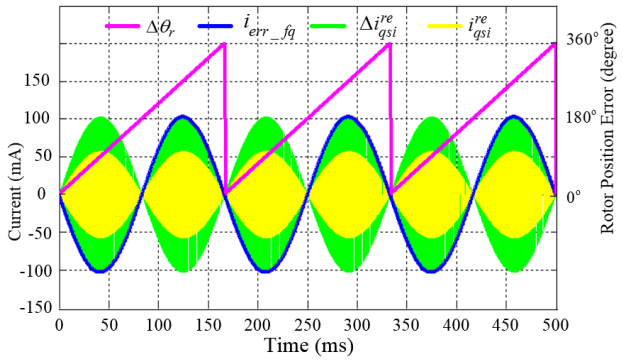

FIGURE 5. Calculation of q-axis induced current error with the field HF voltage injection.

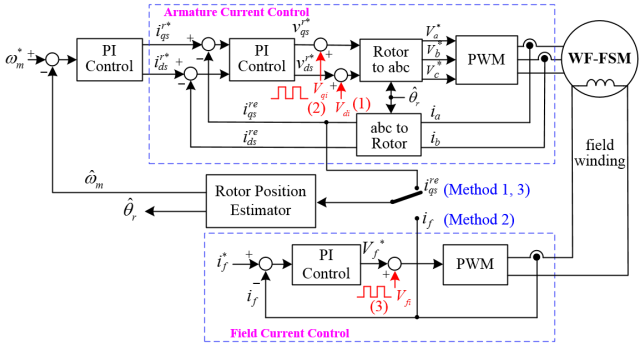

FIGURE 6. Block diagram of the shaft-sensorless control based on the square-wave HF voltage injection.

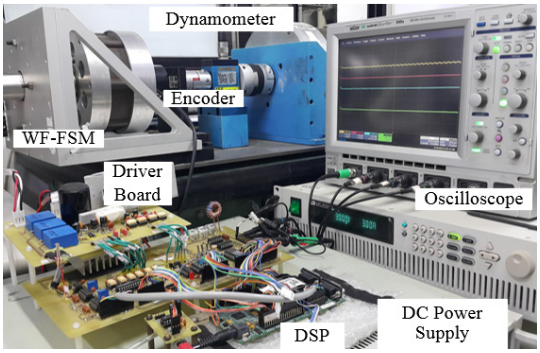

FIGURE 7. Experimental system.

As shown, K_{err_fq} is identical to K_{err_qf} in (19) except that the magnitude is slightly smaller. The dominant parameter for both position error sensitivity factors is the mutual inductance between the armature and field windings.

Figure 5 shows the calculated induced current error versus rotor position error with the field voltage injection. Again, ΔT and V_{fi} are set to the same level as those used in Section III. The estimator shown in Fig. 3 is also used to estimate rotor position with i^{re}_{qsi} as the input to the estimator and i_{err_fq} as the input to the PI controller. i_{err_fq} also has one cycle per electrical period and therefore does not require polarity identification. In the scheme with field voltage injection, the field current did not contain any position error information.

From the analytical and simulation results presented in Sections III–V, the q-axis and the field HF voltage injection schemes are much simpler than the d-axis HF voltage injection scheme because they do not need polarity identification. Moreover, among these three methods, the q-axis HF voltage injection has the highest position error sensitivity.

VI. CONTROL STSTEM

Figure 6 shows the block diagram for the shaft-sensorless control of WF-FSM based on the proposed square-wave HF voltage injection schemes. To compare the performances of the methods presented in the previous sections, the input to the rotor position estimation is set to either i^{re}_{ds}, i^{re}_{qs} or i_f, depending on the type of voltage injection used. The output of the position estimator is motor electrical position and speed. The estimated electrical position is used for the coordinate transformations of the current controller, and the estimated speed is used for the feedback control of the speed controller. For convenience, the proposed d-axis, q-axis, and field HF voltage injection schemes are denoted as **Method 1**, **Method 2**, and **Method 3**, respectively, in Fig. 6 and the subsequent experimental verifications.

VII. EXPERIMENTAL VALIDATIONS

The proposed control schemes were implemented with a TI-TMS320F28335 digital signal processor and verified experimentally. The execution rates for the current and speed control loops were 18.31 and 2.28 kHz, respectively. Fig. 7 shows the experimental system. The WF-FSM was mounted on a dynamometer. A hysteresis brake attached to the rotor shaft delivered the required load torque. An encoder mounted on the same shaft provided the actual rotor position for position error assessments.

A. HF INDUCTANCE

The HF inductances were measured and used to define the injection frequency and voltage level for experimental verification. As shown in (9), there are four inductances relating to the HF model, namely L_{qs}, L_{ds}, L_{mf}, and L_{fs}. Equation (9) can be rewritten by approximating the differences as follows:

$$L_{qs} = \frac{V^r_{qsi}\Delta T}{\Delta i^r_{qsi}} \tag{24}$$

$$V^r_{dsi} = L_{ds}\cdot\frac{\Delta i^r_{dsi}}{\Delta T} + L_{mf}\frac{\Delta i_{fi}}{\Delta T} \tag{25}$$

$$V_{fi} = \frac{3}{2}L_{mf}\frac{\Delta i^r_{dsi}}{\Delta T} + L_{fs}\frac{\Delta i_{fi}}{\Delta T} \tag{26}$$

where all the difference values were measured experimentally. As shown, L_{qs} can be calculated directly using (24) from the incremental voltage and current. However, there are only two equations, (25) and (26), for the other three inductances. Therefore, these inductances could not be calculated directly. Fig. 8 shows the calculation procedures for L_{ds}, L_{mf}, and L_{fs}. Because $L_{ds} \cong L_{qs}$ for this machine, L_{ds} is assumed equal

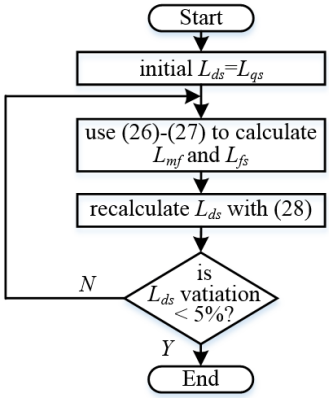

FIGURE 8. Calculation procedures for HF inductances.

toL_{qs} initially, and L_{mf} and L_{fs} can be solved with (25)–(26) simultaneously. Next, L_{ds} is recalculated with the following expression:

$$L_{ds} = \frac{\frac{3L_{mf}}{2}\left(V^r_{dsi} - L_{mf}\left(\frac{\Delta i_{fi}}{\Delta T}\right)\right)}{V_{fi} - L_{fs}\left(\frac{\Delta i_{fi}}{\Delta T}\right)} \tag{27}$$

With the updated L_{ds}, L_{mf} and L_{fs} could again be solved. The calculation procedure is repeated until L_{ds} variation is less than 5% of its previous value. This only took several steps.

The HF inductances for various levels of injection voltage and injection frequency ($f_i = 1/(2\Delta T)$) are shown in Fig. 9. As presented, the variations of all inductances with voltage magnitude were relatively small. Moreover, L_{qs} decreased with the injection frequency, but the variation with frequency is less obvious for the other inductances. Specifically, L_{ds} and L_{fs} reached their minimum values at 2.28 kHz while L_{mf} achieved the maximum value at the same injection frequency. Based on the measured inductances and the analytical results presented in Sections III–V, the maximum induced current is located at 2.28 kHz for all the presented schemes. Therefore, 2.28 kHz and 20 V were used for the injection frequency and voltage in the following experiments to assure reliable current error signal measurements.

B. COMPARISON OF HF INDUCED CURRENT ERROR

Figure 10 presents a comparison of the measured induced current errors of the proposed methods when the motor is at a standstill and the error between the actual rotor position and the estimated position ($\Delta\theta_r$) varied from zero to 360°. The induced current error had two cycles per electrical period for Method 1 and only one cycle per electrical period for Methods 2 and 3. Moreover, the peak of the position error signals i_{err_dq}, i_{err_qf}, and i_{err_fq} were 45, 125, and 90 mA, respectively. The sensitivity factors for Methods 2 and 3 were significantly higher than that of Method 1. These results are consistent with the analysis shown in the previous sections. The difference currents shown in Fig. 8 (b) and (c) appears to be symmetrical, but the difference current Δi^{re}_{qsi} in Fig. 8(a) is apparently asymmetrical for the adjacent half cycles.

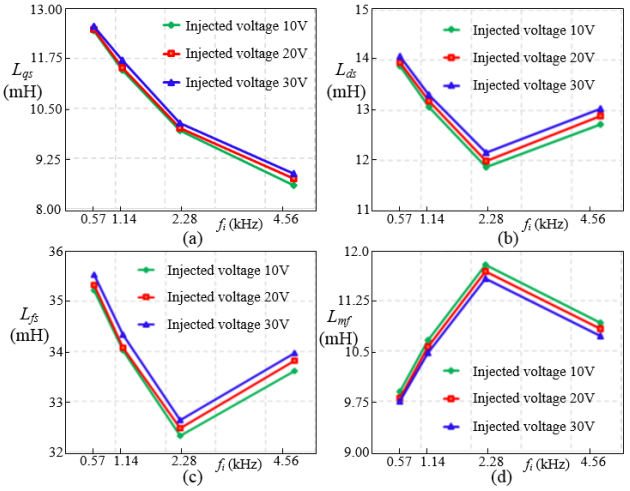

FIGURE 9. Measured incremental inductances, (a) L_{qs}, (b) L_{ds}, (c) L_{fs}, and (d) L_{mf}.

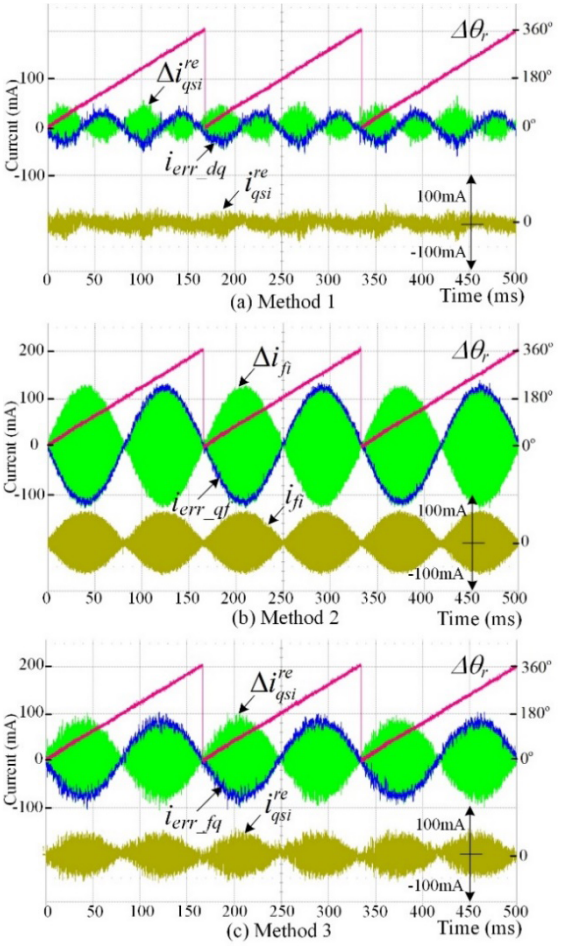

FIGURE 10. Measured HF currents when the machine is at a standstill and the position error varied from zero to 360°.

This property caused DC offset to i_{err_dq}, and consequently added errors to the estimated rotor position.

Figure 11 presents a comparison of the calculated and measured magnitude of the induced current errors for

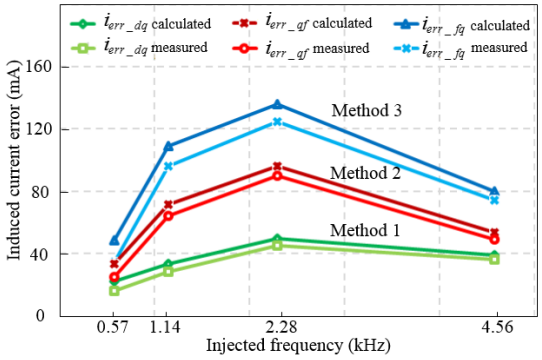

FIGURE 11. Calculated and measured induced current errors when the injection voltage is set at 20 V for various injection frequencies.

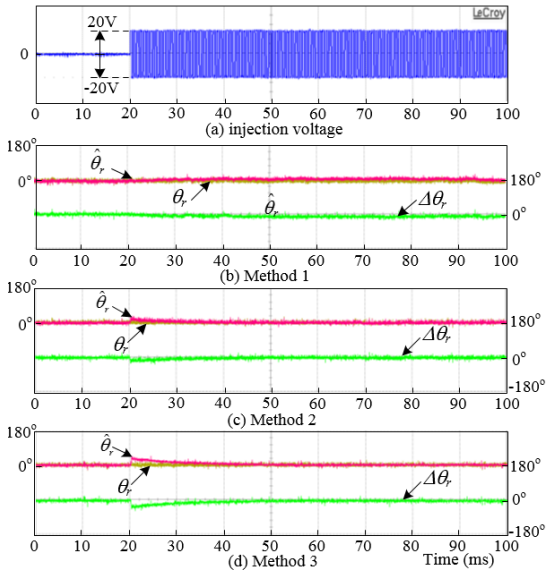

FIGURE 12. Position estimation when the rotor is at 0°.

various injection frequencies when the voltage is set at 20 V. As shown, the maximum induced current error is obtained when the injection frequency is set to 2.28 kHz.

C. COMPARISON OF ROTOR POSITION ESTIMATION

Figures. 12-14 show the initial position estimations using the three presented methods for the rotor stopped at 0, 56, and 236 electrical degrees (°E). The initial estimated position is set to 0° in all the experiments, and the estimator gains are the same for all methods. As presented, the methods tracked the real rotor positions with different settling times. Overall, Method 1 required more settling time than the other two methods because of the lower sensitivity factor for the position error. Moreover, polarity identification extended the settling time to more than 50 ms (Fig. 14). Conversely, Methods 2 and 3 required only 10-15 ms to reach the actual rotor position due to the higher sensitivity factor for the position error and because polarity identification is not required.

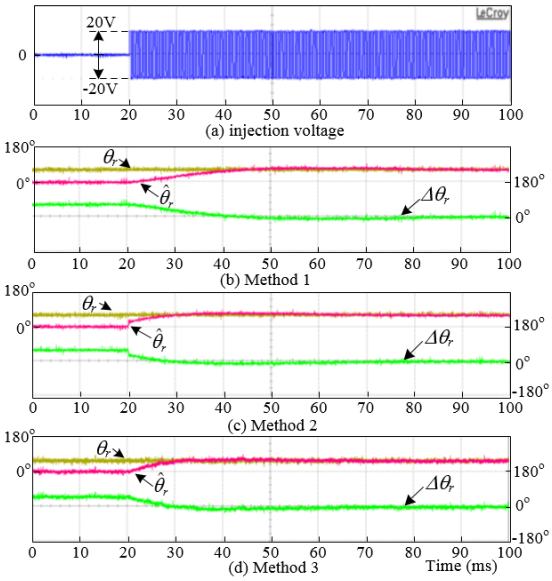

FIGURE 13. Position estimation when the rotor is at 56°.

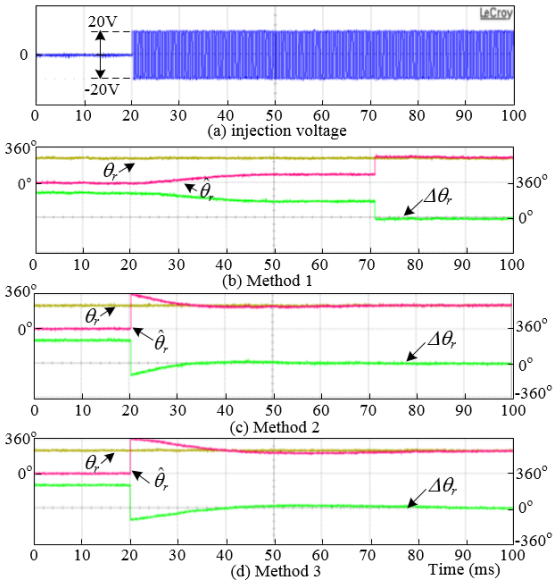

FIGURE 14. Position estimation when the rotor is at 236°.

D. COMPARISON OF DYNAMIC RESPONSE

Figure 15 compares the dynamic response of shaft-sensorless control under no load and 100% load using the proposed methods. The external load was applied when the motor was running at constant speed. As shown, all the methods displayed satisfactory dynamic performances. However, the position errors are relatively different. As presented in Fig. 15(a), the position error for Method 1 is approximately 18° without load and dropped to 6° after the load is applied. The high estimated position error is due to the low sensitivity of the position error signal i_{err_dq}. Furthermore, the asymmetric HF current Δi_{qsi}^{re} also contributed to the error of the estimated position. The asymmetric level related to the load

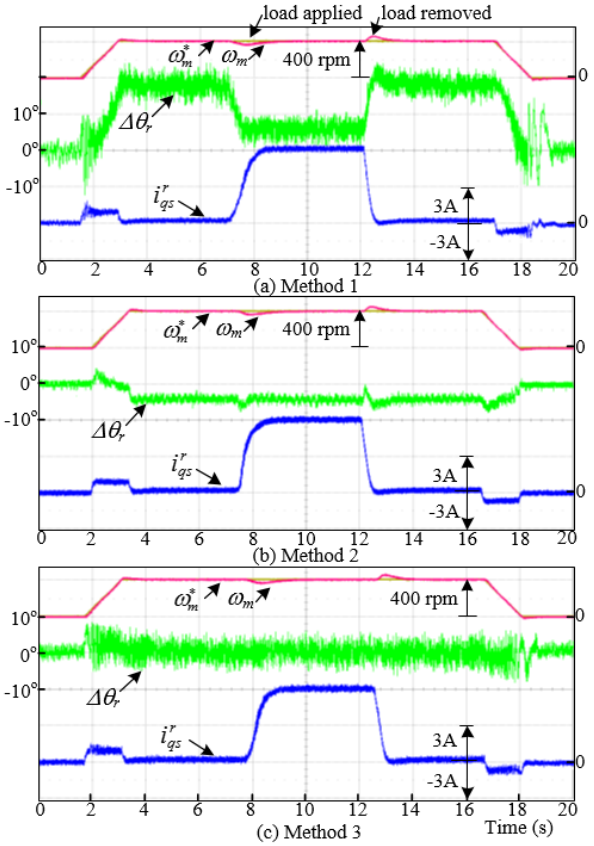

FIGURE 15. Responses of shaft-sensorless speed control, 100% load is applied when the motor is running at a constant speed.

torque. A higher q-axis current reduced the asymmetric level of Δi^{re}_{qsi}, and consequently, reduced the estimation errors.

As shown in Fig. 15(b), the position error for Method 2 is 4°, 5°, and 8° during acceleration, constant speed, and deceleration, respectively. The position error ripple is low, approximately 4°, and is insensitive to load variation. Fig. 15(c) presents the performance of Method 3. As presented, the position error is between 5° and −5° when the motor is running at a constant speed, with or without load. During acceleration and deceleration, the error is slightly higher, approximately 8°. The position error ripple is slighter higher than that of the other two methods.

In sum, both the q-axis and field voltage injection (Methods 2 and 3) exhibited excellent performance in the experimental conditions. However, the q-axis injection voltage using Method 2 ultimately limited the operating speed range of the machine. Therefore, Method 3 is more advantageous for high-speed operations because the HF voltage is injected into the field winding.

VIII. CONCLUSON

This study investigated three HF square-wave voltage injection schemes for shaft-sensorless control of WF-FSM drives. Table 2 summarizes the performance comparisons of these schemes. The experimental results revealed that all three methods tracked rotor position relatively well. However, the scheme that utilized the mutual inductance of the armature windings by injecting voltage at the d-axis and processing q-axis induced current exhibited the highest position errors due to its low sensitivity of the position error signal and asymmetrical differential HF current. Moreover, this scheme also required polarity identification as with conventional PMSMs. The other two schemes utilized the mutual inductance between the armature and phase windings (i.e., injected HF voltage into the armature winding and processed the induced current in the field winding, or vice versa). They are more robust than the other method due to the high sensitivity of the induced current errors and because they are independent of the saliency of the machine. Moreover, their implementations are simpler because no polarity identification is required. The scheme with voltage injection at the field winding (Method 3) had an additional advantage for high-speed operations because field voltage did not increase with motor speed.

TABLE 2. Comparison of the three methods.

Specification	Method 1	Method 2	Method 3
Strength of induced current error	-	+	0
Noise of induced current error	-	+	0
Estimated position error	-	+	+
Polarity identification	-	+	+
High speed operation	-	-	+

- : Bad 0 : Fair + : Good

REFERENCES

[1] Y.-S. Jeong, R. D. Lorenz, T. M. Jahns, and S.-K. Sul, "Initial rotor position estimation of an interior permanent-magnet synchronous machine using carrier-frequency injection methods," *IEEE Trans. Ind. Appl.*, vol. 41, no. 1, pp. 38–45, Jan. 2005.

[2] F. Gabriel, F. De Belie, X. Neyt, and P. Lataire, "High-frequency issues using rotating voltage injections intended for position self-sensing," *IEEE Trans. Ind. Electron.*, vol. 60, no. 12, pp. 5447–5457, Dec. 2013.

[3] S.-I. Kim, J.-H. Im, E.-Y. Song, and R.-Y. Kim, "A new rotor position estimation method of IPMSM using all-pass filter on high-frequency rotating voltage signal injection," *IEEE Trans. Ind. Electron.*, vol. 63, no. 10, pp. 6499–6509, Oct. 2016.

[4] Z. Zhu, A. Almarhoon, and P. Xu, "Improved rotor position estimation accuracy by rotating carrier signal injection utilizing zero-sequence carrier voltage for dual three-phase PMSM," *IEEE Trans. Ind. Electron.*, vol. 64, no. 6, pp. 4454–4462, Jun. 2017.

[5] S. Kim, J.-I. Ha, and S.-K. Sul, "PWM switching frequency signal injection sensorless method in IPMSM," *IEEE Trans. Ind. Appl.*, vol. 48, no. 5, pp. 1576–1587, Sep./Oct. 2012.

[6] J. M. Liu and Z. Q. Zhu, "Novel sensorless control strategy with injection of high-frequency pulsating carrier signal into stationary reference frame," *IEEE Trans. Ind. Appl.*, vol. 50, no. 4, pp. 2574–2583, Jul./Aug. 2014.

[7] X. Luo, Q. Tang, A. Shen, and Q. Zhang, "PMSM sensorless control by injecting HF pulsating carrier signal into estimated fixed-frequency rotating reference frame," *IEEE Trans. Ind. Electron.*, vol. 63, no. 4, pp. 2294–2303, Apr. 2016.

[8] Y.-D. Yoon, S.-K. Sul, S. Morimoto, and K. Ide, "High-bandwidth sensorless algorithm for AC machines based on square-wave-type voltage injection," *IEEE Trans. Ind. Appl.*, vol. 47, no. 3, pp. 1361–1370, May/Jun. 2011.

[9] D. Kim, Y.-C. Kwon, S.-K. Sul, J.-H. Kim, and R.-S. Yu, "Suppression of injection voltage disturbance for high-frequency square-wave injection sensorless drive with regulation of induced high-frequency current ripple," *IEEE Trans. Ind. Appl.*, vol. 52, no. 1, pp. 302–312, Jan. 2016.

[10] S.-C. Yang, S.-M. Yang, and J.-H. Hu, "Design consideration on the square-wave voltage injection for sensorless drive of interior permanent-magnet machines," *IEEE Trans. Ind. Appl.*, vol. 64, no. 1, pp. 159–168, Jan. 2017.
[11] S.-C. Yang and Y.-L. Hsu, "Full speed region sensorless drive of permanent-magnet machine combining saliency-based and back-EMF-based drive," *IEEE Trans. Ind. Electron.*, vol. 64, no. 2, pp. 1092–1101, Feb. 2017.
[12] J. Holtz, "Acquisition of position error and magnet polarity for sensorless control of PM synchronous machines," *IEEE Trans. Ind. Appl.*, vol. 44, no. 4, pp. 1172–1180, Jul./Apr. 2008.
[13] D. Raca, M. C. Harke, and R. D. Lorenz, "Robust magnet polarity estimation for initialization of PM synchronous machines with near-zero saliency," *IEEE Trans. Ind. Appl.*, vol. 44, no. 4, pp. 1199–1209, Jul. 2008.
[14] P. Xu and Z. Q. Zhu, "Initial rotor position estimation using zero-sequence carrier voltage for permanent-magnet synchronous machines," *IEEE Trans. Ind. Electron.*, vol. 64, no. 1, pp. 149–158, Jan. 2017.
[15] J. Choi, I. Jeong, S. Jung, and K. Nam, "Sensorless control for electrically energized synchronous motor based on signal injection to field winding," in *Proc. Ind. Electron. Soc. Conf.*, 2013, pp. 3120–3129.
[16] Y. Tang, J. J. H. Paulides, T. E. Motoasca, and E. A. Lomonova, "Flux-switching machine with DC excitation," *IEEE Trans. Magn.*, vol. 48, no. 11, pp. 3583–3586, Nov. 2012.
[17] H. Q. Nguyen, J. Y. Jiang, and S. M. Yang, "Design of a 12-slot 7-pole wound-field flux switching motor for traction applications," in *Proc. Int. Ind. Tech. Conf.*, 2016, pp. 1275–1280.
[18] S.-M. Yang, J.-H. Zhang, and J.-Y. Jiang, "Modeling torque characteristics and maximum torque control of a three-phase, DC-excited flux-switching machine," *IEEE Trans. Magn.*, vol. 52, no. 7, Jul. 2016, Art. no. 8104204.
[19] T.-C. Lin, Z.-Q. Zhu, K. Liu, and J. M. Liu, "Improved sensorless control of switched-flux permanent-magnet synchronous machines based on different winding configurations," *IEEE Trans. Ind. Electron.*, vol. 63, no. 1, pp. 123–132, Jan. 2016.
[20] H.-Q. Nguyen and S.-M. Yang, "Comparison of high frequency voltage injection methods for shaft sensorless control of wound-field flux switching machine," in *Proc. Int. Power Electron. Conf.*, 2018, pp. 3426–3430.
[21] S.-C. Yang, S.-M. Yang, and J.-H. Hu, "Robust initial position estimation of permanent magnet machine with low saliency ratio," *IEEE Access*, vol. 5, pp. 2685–2695, Feb. 2017.

HONG QUAN NGUYEN was born in Hanoi, Vietnam. He received the bachelor's degree in electrical engineering from the Hanoi University of Science and Technology, Hanoi, in 2012, and the M.S. degree in electrical engineering and computer science from the National Taipei University of Technology, Taipei, Taiwan, in 2014, where he is currently pursuing the Ph.D. degree with the Department of Electrical Engineering.

His research interests include motor design, motor drives, and control techniques without shaft position sensors.

SHENG-MING YANG (M'86) was born in Taipei, Taiwan. He received the M.S. and Ph.D. degrees from the University of Wisconsin–Madison in 1985 and 1989, respectively. From 1989 to 1992, he was a Development Engineer with Unico Inc. From 1992 to 1995, he was a Principal Engineer with the Corporate Technology Center, A. O. Smith Corporation, Milwaukee, WI, USA. In 1995, he joined the Department of Mechanical and Electro-Mechanical Engineering, Tamkang University, Taiwan, as a Professor. Since 2007, he has been with the Department of Electrical Engineering, National Taipei University of Technology, Taiwan. His research interests are ac and dc motor drives and control.